

Searching for Lensed Gravitational Waves from Compact Binary Coalescences

Interim Report 2

Li Ka Yue Alvin¹

Mentors: Alan J. Weinstein² and Surabhi Sachdev²

¹Department of Physics, The Chinese University of Hong Kong

²LIGO Laboratory, California Institute of Technology

LIGO SURF 2018 Program, California Institute of Technology

Date : 3rd August, 2018

Einstein's general relativity predicts the radiation of gravitational waves when masses accelerates, for instance, as the components of a binary black hole system orbit each other. This was confirmed when LIGO (The Laser-Interferometry Gravitational-wave Observatory) made the first detection of gravitational waves from a binary black hole merger on 14 September 2015. The success of gravitational waves detection opens a new window for scientists to study the Universe. In Einstein's general theory of relativity, it is also predicted that light rays bend when passing by masses in spacetime, a phenomenon known as gravitational lensing. As a manifestation of Einstein's equivalence principle [1], everything in motion, independent of their nature, is gravitationally lensed in the same way. In such sense, gravitational waves will also be lensed, resulting in multiple signals which differ in arrival times and amplitudes. Since the amplitudes of such signals may differ, there are cases that they are not identified as signals. In this research, we aim to search for lensed signals of the binary black hole signals detected by LIGO. We generate templates of possible lensed gravitational wave signals for detected events by simulating gravitational wave signals as observed by LIGO. Our major objective is to make use of those templates to re-identify possible lensed signals which may have insufficiently high signal-to-noise ratio to be distinguishable from detector noise. We will further attempt to infer the intrinsic properties of the gravitational lenses from the lensed gravitational wave signals identified.

I. Introduction and Motivation

With the successful detections of gravitational waves [2]–[7] over the past few years, we have already verified the existence of gravitational waves predicted by Albert Einstein's general theory of relativity in 1915 [8]. Therefore, it is now the right time to test the other properties of gravitational waves as General Relativity predicts, and in this project, our main focus is gravitational lensing. In particular, we aim to search for lensed gravitational wave signals of confirmed LIGO events from compact binary coalescences. Our major goal is to set up and test a methodology for re-identify possible lensed candidates which are initially indistinguishable from the background. We will then try to infer the intrinsic properties of the gravitational lenses by making use of the identified lensed gravitational wave signals.

In this report, Section II provides background information on the research. Section III summarizes the previous work. Section IV discusses the work progress and the problems and challenges encountered so far. Section V describes the upcoming plans for the research and the anticipated challenges. Finally, Section VI illustrates the work plan for the research.

II. Background

A. Properties of Gravitational Waves

According to Albert Einstein's general theory of relativity in 1915 [8], the Universe can be perceived as a fabric of spacetime. Masses like black holes and neutron stars on this fabric produce spacetime curvature [9]. When masses move in spacetime, they cause ripples like water waves generated when one throws a stone into water. Such ripples are known as **gravitational waves**. In this project we focus on four fundamental properties for gravitational waves as predicted by General Relativity, namely their speed, polarization, weak interaction with matter and ability to be lensed gravitationally.

The speed of gravitational waves is predicted by General Relativity to be the same as the speed of light c in vacuum [10]. This has been experimentally confirmed by the detection of gravitational wave from the neutron star inspiral GW170817 in 2017, which constrained the difference between the speed of light and the speed of gravitational wave to between -3×10^{-15} and $+7 \times 10^{-16}$ [11] times the speed of light c .

For the polarization of gravitational waves, as discussed in Ref. [12], we imagine placing a circular ring of test masses on the $x - y$ plane with its center coinciding with the origin. If we assume there exists a transverse - traceless (TT) gravitational wave propagating in the z -direction, then

the effect of such gravitational wave is constrained to be on the $x - y$ plane only. Under the influence of the wave, the test masses ring can exhibit two orthogonal deformation modes.

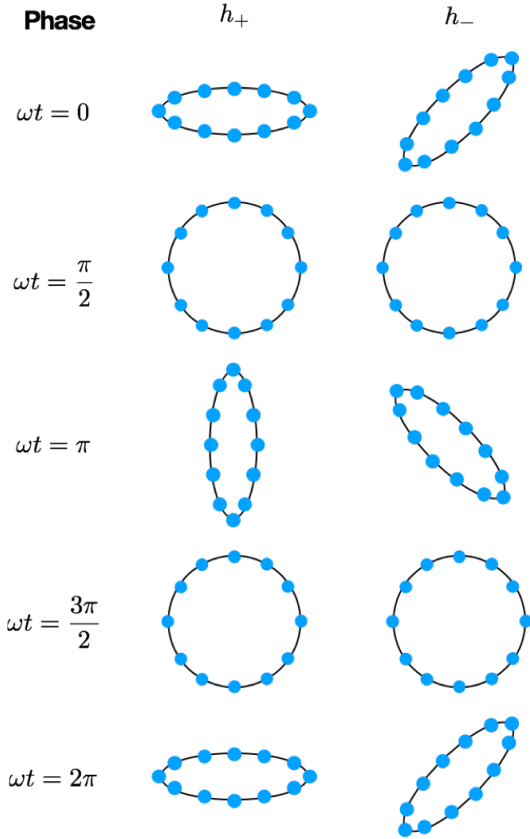


Fig. 1. Two orthogonal deformation modes within one period of the test mass ring in response to a TT-gravitational wave. The upper row refers to the plus polarization (denoted by +) and the lower row refers to the cross polarization (denoted by \times) of the gravitational wave. Image reproduced from [12].

As shown in Figure 1, when a **plus (+) polarized** gravitational wave passes through our ring of test masses, the ring is stretched along the y -direction and then along the x -direction into an ellipse of the same area as the original circle throughout one period. On the other hand, if the gravitational wave passing through is **cross (\times) polarized** instead, the ring will be stretched along the $y = x$ and $y = -x$ line in a similar way as for plus (+) polarized gravitational wave. We can see that gravitational waves can be polarized in two particular modes, namely the plus (+) polarization, and cross (\times) polarization. The effect of stretching and shrinking of proper lengths between test masses in the ring by polarized gravitational waves is applied to the detection of gravitational waves. In particular, detectors including LIGO and VIRGO detect gravitational waves using interferometry.

B. Detection of Gravitational Waves

A schematic overview of the gravitational wave detector used by LIGO is shown in Figure 2 [13]. It is a Michelson

interferometer consisting of two arms, each of 4 km long. A laser beam is incident on a beam splitter, which splits the incident laser beam into two beams propagating along the two arms of the interferometer. At the end of the arm, a mirror reflects the beams which then rejoin at the beam splitter and is finally collected by a photodetector to observe the interference pattern.

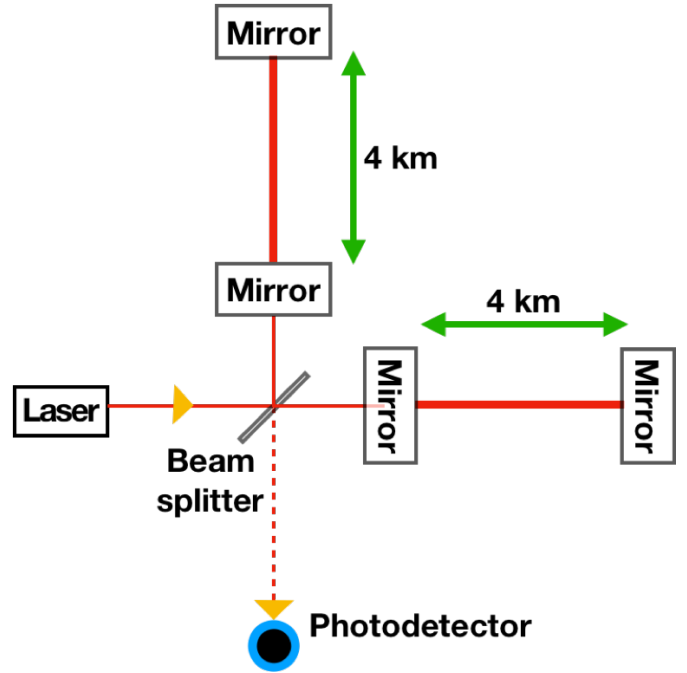


Fig. 2. A schematic overview of the gravitational wave detector used by LIGO. Image reproduced from [13].

The interference of the two laser beams is set to be destructive at the photodetector. Alternatively, when there are alterations to the lengths of the arms which cause a path difference between the two laser beams, a constructive interference pattern will be observed. The change in arm lengths is not necessarily caused by gravitational waves because there is also noise which can cause such effect. These noises include seismic noises, thermal noises, gravity-gradient noises and quantum noises [14].

In order to detect gravitational waves, we must constrain ourselves to those which have a sufficiently large perturbation to spacetime. Typically, we focus on four types of gravitational waves, namely Continuous Waves, Stochastic Waves, Bursts and Compact Binary Coalescences, the last one is the focus of this research. When two compact objects, for instance, neutron stars and/or black holes, orbit about their common center-of-mass, they will **inspiral** due to loss of orbital energy by means of gravitational radiation, then **merge** into a single object which then **rings down**. This sequence, "inspiral-merger-ringdown", is referred to as "coalescence". Among the four mentioned types of gravitational waves, Compact Binary Coalescences are sources of gravitational waves with well modelled waveforms compared to other kinds of gravitational wave sources, and

hence one can use a technique called **matched filtering** to search for such signals.

We now outline the major steps in analyzing gravitational-wave data [12]. Currently, matched filtering is a method to distinguish the weak gravitational wave signals from the detector noise fluctuations. The principle of matched filtering is to slide templates of an expected waveform from an astrophysical event across the received data and look for a strong cross-correlation between the two.

We denote $s(t)$ as the signal received from a detector, $n(t)$ as the background noise and $h(t)$ as the gravitational wave signal (if it exists). $s(t)$ is the sum of $n(t)$ and $h(t)$, that is

$$s(t) = n(t) + h(t). \quad (1)$$

If we have a filter $P(t)$, we may define

$$\hat{s} = \int s(t)P(t)dt. \quad (2)$$

We denote $\langle S \rangle$ and N as the expectation value and root mean square value of \hat{s} if a gravitational wave signal is included in the data respectively. Then we have

$$\begin{aligned} \langle S \rangle &= \int \langle s(t)P(t) \rangle dt \\ &= \int \langle (n(t) + h(t))P(t) \rangle dt \\ &= \int \langle h(t)P(t) \rangle dt \\ &= \int h\tilde{h}(f)\tilde{P}^*(f)df, \end{aligned} \quad (3)$$

where we have taken $\langle n(t) \rangle = 0$ (since the noise is assumed to be random and gaussian) and the tilde (\tilde{A}) denotes the Fourier-transformed function of A .

Also, if $h(t) = 0$, we have

$$\begin{aligned} N^2 &= \langle \hat{s}^2 \rangle - \langle \hat{s} \rangle^2 \\ &= \langle \hat{s}^2 \rangle \\ &= \int \int P(t)P(t')\langle n(t)n(t') \rangle dt dt' \\ &= \frac{1}{2} \int S_n(f)|\tilde{P}(f)|^2 df, \end{aligned} \quad (4)$$

where $S_n(f)$ denotes the power spectral density. We can therefore define **signal-to-noise ratio (SNR)** as

$$\begin{aligned} \rho &= \frac{\langle S \rangle}{N} \\ &= \frac{\int h\tilde{h}(f)\tilde{P}^*(f)df}{\sqrt{\int \frac{1}{2}S_n(f)|\tilde{P}(f)|^2 df}}. \end{aligned} \quad (5)$$

Furthermore, we define the inner product between two functions $x(t)$ and $y(t)$ to be:

$$\langle x, y \rangle = \Re \left(\int_{-\infty}^{\infty} \tilde{x}^*(f)\tilde{y}(f) \frac{1}{2}S_n(f) df \right). \quad (6)$$

Consequently, we can have equation (5) simplified as

$$\rho = \frac{\langle d, h \rangle}{\sqrt{\langle h, h \rangle}}, \quad (7)$$

where d is the data received in the detector. With an optimal matched filter $P(t)$, and provided that the identical gravitational wave signal can be seen in coincidence between two or more detectors, LIGO detectors can detect inspiral signals with a network SNR $\rho_{\text{net}} > 8$ [15]. The network SNR for two or more detectors is simply calculated by adding the SNR of individual detectors in quadrature, that is

$$\rho_{\text{net}}^2 = \sum_i \rho_i^2, \quad (8)$$

where the index i runs over the individual detectors [12].

In reality, the rate of gravitational wave events occurring is expected to as low as about a few per year [14]. To avoid mistaking large and infrequent detector noise fluctuations mimicking events as signals, we need to find out the **false alarm rate (FAR)**, which is how often an abnormal noise signal mimicking event can be measured. The smaller the FAR is, the more plausible the candidate is a real astrophysical event. The FAR for any signal is estimated by [16]

$$\text{FAR} = \frac{N}{\sum_i T_i}, \quad (9)$$

where N is the total number of background triggers similar to the one which we consider as a real signal, and T_i is the analyzed time interval in the i^{th} background trial.

C. Gravitational Lensing

As predicted by General Relativity, since masses can curve spacetime, the path of a light ray from a source can be bent and deflected before reaching the observer (See Figure 3). Such effect is known as gravitational lensing, in the sense that it is similar to light rays being bent by optical lenses, but in this case the ‘‘lenses’’ are masses instead. In particular, since a source emits light rays in all direction, light rays propagating along different directions are bent differently and may, therefore, form multiple images. The images can vary in arrival time and amplitudes.

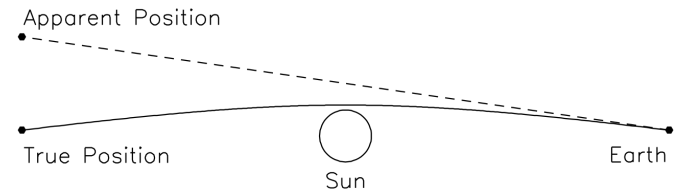


Fig. 3. Light rays from a source are bent because of a gravitational lens in between the source and the observer. Image from [17].

In fact, all electromagnetic waves, as well as all gravitational waves, can be gravitationally lensed in the same way, and this phenomenon has been observed on astronomical scales for light of all wavelengths. However, the study of

gravitational lensing of light encounters difficulties from the blocking of light by dust clouds in the Universe, as well as the large noise which screened the light signals [18]. General relativity also predicts that gravitational waves, having a similar nature as light, can also be lensed gravitationally, producing multiple signals, and same as light, is achromatic. In contrast to light, gravitational waves are not disturbed by the dust clouds between the source and observing point.

Over the past two years, more than six gravitational wave detections have been successfully made [2]–[7], which have confirmed the prediction of the existence of gravitational waves. Among the four predicted fundamental properties of gravitational waves, which are their speed, polarization, weak interaction with matter and ability to be lensed gravitationally, that we mentioned at the very beginning of Section II, we are only left with the last one - ability to be gravitationally lensed untested. Therefore, it is now the right time for us to start searching for lensed gravitational wave signals so as to test the final property of gravitational wave predicted from general relativity.

Due to lensing, there are time delays among the waves of images. In the discussion for electromagnetic waves, there are two major contribution to the delay, namely refraction and gravitational time delay. Gravitational lensing occurs when light rays pass through spacetime perturbed by masses. This will form multiple signals which differ in amplitude and time of arrival. The difference in arrival time is due to 1) The path lengths travelled from the images to the observer vary, and 2) The effective speed of light can be different under the influence of a refractive index larger than one, resulting in arrival time delay.

The same thing happens with gravitational waves, except that their weak interaction with matter means that the refractive index is negligibly different from one. Therefore, the only crucial effect to account for is the geometric effect, which causes both magnification and time delay of lensed signals. An important point to note here is that there is no dispersion, and hence the geometric lensing is achromatic. That is to say, it affects all frequency components of the wave in exactly the same way.

In the derivations below, for cosmological distances, they are referred to as the angular diameter distances. As shown in Figure 4, the angular diameter distances from the observer to the lens and the source are given by D_L and D_S respectively, and that from the source to the lens is D_{LS} . When we compare the path difference between the unperturbed ray (dotted line between the observer and the source in figure 4), that is when the lens is absent, and the lensed ray (solid lines between the observer and the source), we have [19]

$$\vec{\xi} = \frac{D_L D_{LS}}{D_S} (\vec{\theta} - \vec{\theta}_S), \quad (10)$$

where ξ is the separation between the two rays at the lens, $\vec{\theta}$ is the two-dimensional angle between the horizontal of the observer and the point where the gravitational waves strike

the lens, and $\vec{\theta}_S$ is the angle between the horizontal of the observer and the source.

With this, we have the geometrical path difference $\Delta\lambda$ between the unperturbed ray and lensed ray is given by

$$\Delta\lambda = \frac{\xi(\vec{\theta} - \vec{\theta}_S)}{2}. \quad (11)$$

Finally, the geometrical time delay Δt due to gravitational lensing is given by

$$\Delta t = (1 + z_d) \frac{D_L D_{LS}}{2D_{SC}} (\vec{\theta} - \vec{\theta}_S)^2, \quad (12)$$

where z_d denotes the gravitational redshift. From the calculation of the time delay, we are able to infer the distance of the lens from the observer.

For gravitationally lensed gravitational wave signals, the lensed waveform has an amplitude $h_{+,x}^{\text{lensed}}(f)$ given by [20], [21]

$$h_{+,x}^{\text{lensed}}(f) = F(\omega, y) h_{+,x}^{\text{unlensed}}(f), \quad (13)$$

where $h_{+,x}^{\text{unlensed}}(f)$ denotes the amplitude of the unlensed gravitational waves, and $F(\omega, y)$ is the amplification function given by

$$F(\omega, y) = \exp \left[\frac{\pi\omega}{4} + i\frac{\omega}{2} \left(\ln \left(\frac{\omega}{2} \right) - \frac{\sqrt{y^2 + 4} - y}{4} \right) + \ln \left(\frac{\sqrt{y^2 + 4} + y}{2} \right) \right] \Gamma \left(1 - \frac{i}{2}\omega \right) \times {}_1F_1 \left(\frac{i}{2}\omega, 1; \frac{i}{2}\omega y^2 \right), \quad (14)$$

where $h_{+,x}^{\text{lensed}}(f)$ is the waveform without lensing, Γ is the complex gamma function, ${}_1F_1$ is the confluent hypergeometric function of the first kind, $\omega = 8\pi M_{Lz} f$; $M_{Lz} = M_L(1 + z_L)$ is the redshifted lens mass, $y = \frac{D_L S}{\Xi_0 D_S}$ is the source position, $\Xi_0 = \left(\frac{4M_L D_L D_{LS}}{D_S} \right)^{\frac{1}{2}}$ is a normalisation constant, and M_L and z_L are the lens mass and redshift respectively. From finding the amplitude of the lensed gravitational waves, we can infer both the mass M_L and the position of the lens.

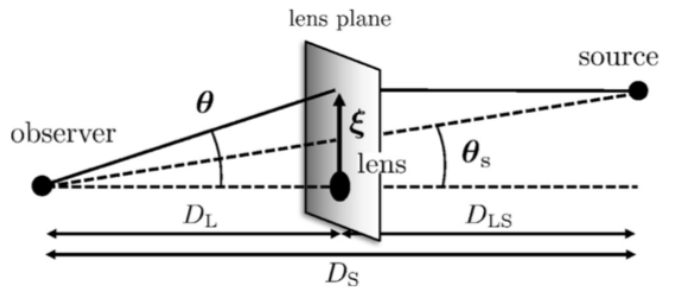


Fig. 4. In this figure, D_L denotes the distance between the lens and the observer, D_S denotes the distance between the observer and the image, D_{LS} denotes the distance between the lens and the image, $\vec{\theta}$ denotes the two dimensional angle between the observer and lensing point, and θ_s denotes the two dimensional angle between the source and the observer. Note that θ and θ_s are both two-dimensional angles. Image from [19].

Consider a point mass lens, particularly for compact objects like black holes or stars. In the geometrical optics limit ($f \gg M_{Lz}^{-1}$) from the equation above, we have [21]

$$F(\omega, y) = |\mu_+|^{1/2} - i|\mu_-|^{1/2} e^{2\pi i f \Delta t_d}, \quad (15)$$

where the magnification of each image is

$$\mu_{\pm} = \frac{1}{2} \pm \frac{(y^2 + 2)}{2y\sqrt{y^2 + 4}}, \quad (16)$$

and the time delay between the double images is

$$\Delta t_d = 4M_{Lz} \left[\frac{y\sqrt{y^2 + 4}}{2} + \ln \left(\frac{\sqrt{y^2 + 4} + 4}{\sqrt{y^2 + 4} - y} \right) \right]. \quad (17)$$

The typical time delay for the point mass lens is therefore $2 \times 10^3 s \times \left(\frac{M_L}{10^8 M_{\odot}} \right)$. Furthermore, for gravitational waves from coalescence of super massive black holes of mass $10^4 - 10^7 M_{\odot}$ under the lensing effect of a point mass lens of mass in the range $10^6 - 10^9 M_{\odot}$, then the typical time delay will be $10 - 14s$ [21]. Therefore, for gravitational waves from blackholes of masses lower than $10^4 M_{\odot}$, we would expect a time delay in the range $10^1 - 10^3 s$.

III. Previous Work

A. GstLAL search pipeline

This research is based on the use of GstLAL search pipeline. Figure 5 shows the schematic flow of the pipeline. Before the start of SURF period, the working scheme of the pipeline has been studied and GstLAL search practice has been run.

B. Searching for possible lensed candidates for GW150914 in O1 and O2 using LALInference posterior data

We make use of LALInference software library [23] posterior data analysis of the event GW150914. The following table shows the posterior estimation of the parameters of the two black holes involved in GW150914:

Parameter	Maximum Posteriori (maP)	Variation (σ)
$m_{1,source}$	$32.9M_{\odot}$	$4.9M_{\odot}$
$m_{2,source}$	$13.7M_{\odot}$	$3.5M_{\odot}$
$a_{1,z}$	-0.618	0.218
$a_{2,z}$	0.083	0.243

where $m_{1,source}$, $m_{2,source}$, $a_{1,z}$ and $a_{2,z}$ are the respective masses and components of spins aligned with the orbital angular momentum of the binary blackhole system of the two black holes in GW150914 evaluated by the LALInference library. Using the information, we search for triggers throughout O1 and O2 with masses and spins within 3 and 4 sigmas from the maP of GW150914 which are regarded as possible lensed candidates for the event. Figure 6 to 9 show the search results for O1 and O2 within 3 sigma range and 4 sigma range. Note that μ on the y-axis refers to the

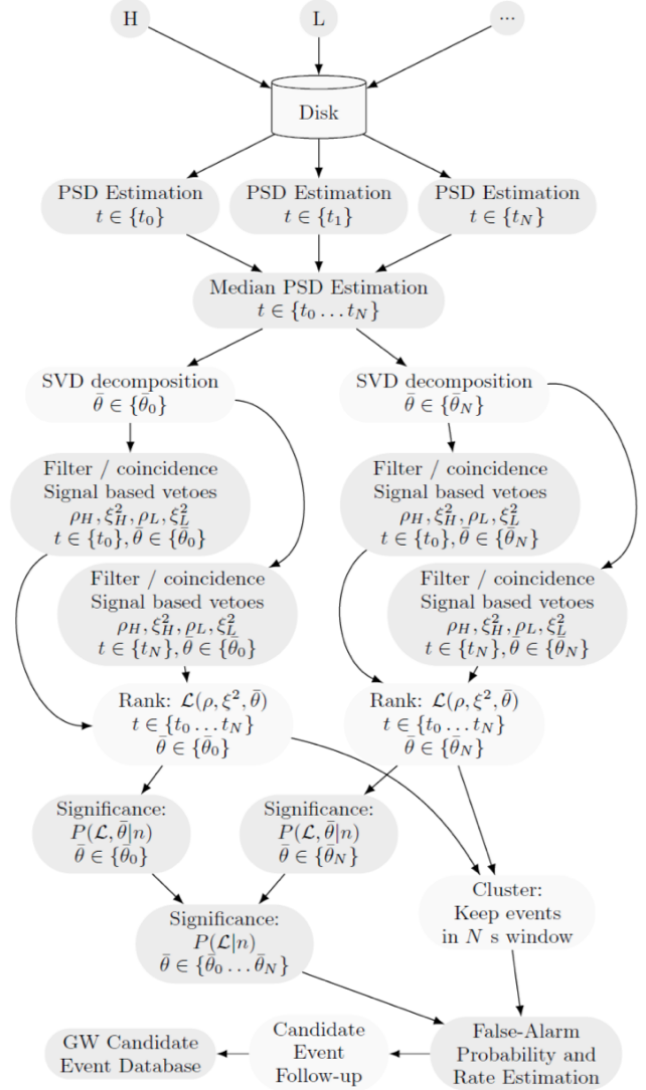


Fig. 5. A schematic flow of the GstLAL search pipeline. Image from [22].

magnification of the triggers comparing to GW150914, which is evaluated by:

$$\mu = \frac{\text{Signal-to-noise ratio of found trigger}}{\text{Signal-to-noise ratio of GW150914}}, \quad (18)$$

and the relative time delay on the x-axis refers to the time delay of the found triggers relative to the geocentric arrival time of GW150914, which is $1126259462s$ [2] (The corresponding UTC time is 2015-09-14 09:50:45). The colours of the dots indicate the likelihood, a measure of the distinguishability of the event from the detector noise, of the triggers.

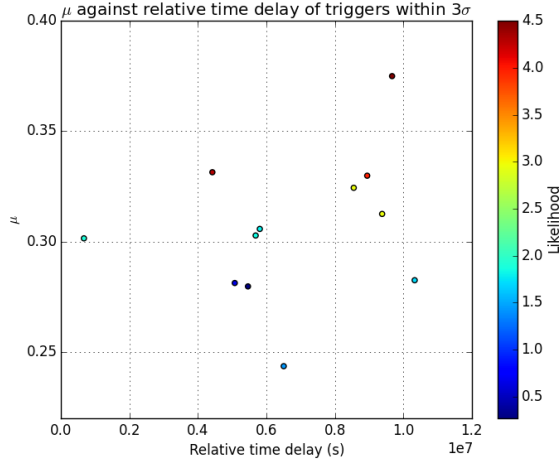


Fig. 6. Searched triggers in O1 with parameters within 3 sigma range from GW150914.

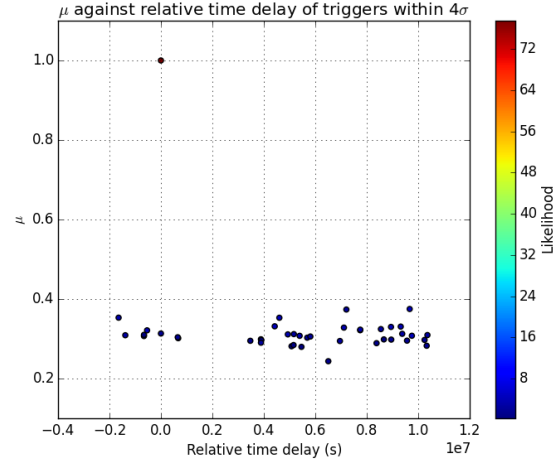


Fig. 8. Searched triggers in O1 with parameters within 4 sigma range from GW150914. Note that the detected GW150914 event is visible at relative time delay = 0 and $\mu = 1$

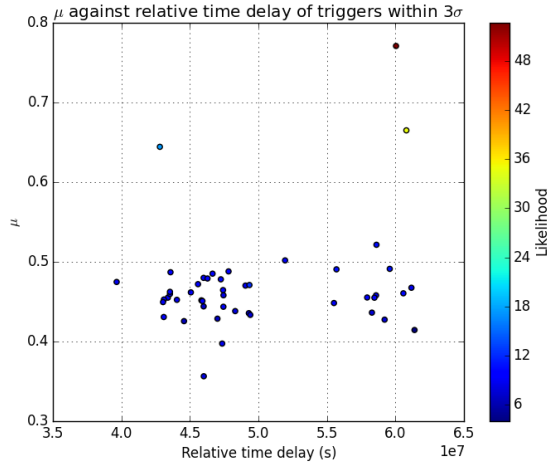


Fig. 7. Searched triggers in O2 with parameters within 3 sigma range from GW150914.

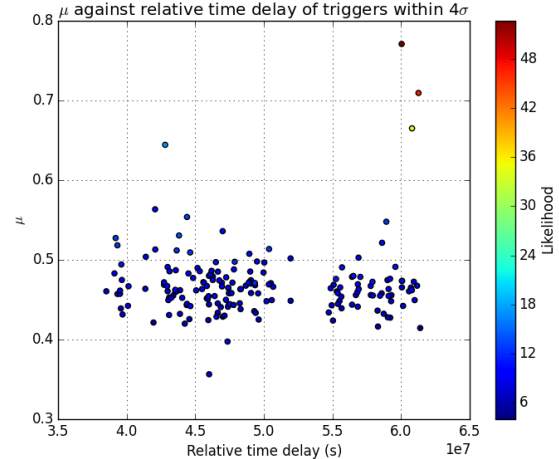


Fig. 9. Searched triggers in O2 with parameters within 4 sigma range from GW150914.

Problems

We note that the trigger, which is a candidate event where the SNR $\rho(t)$ peaks in time above a certain threshold, corresponding to GW150914, which should have $\mu = 1$ and Relative time delay = 0, does not show up in the 3 sigma range plot in O1, and it only shows up when we loosen the range to 4-sigma. This is due to the inconsistency of data used between LALInference and GstLAL. In fact, LALInference is designed to accurately infer the parameters of the source, while GstLAL is not. Therefore, their results are not completely agreeing with each other, leading to the absence of GW150914 in the 3-sigma plot.

Also, we are aware that the signal-to-noise ratio (SNR) evaluated in both O1 and O2 may have discrepancies since the background noise is varying every moment. Initially, we proposed looking into the power spectral density in O1 and O2 to link the SNRs, but we decided to do better and hence

this method is called off.

C. Searching for possible lensed candidates for GW150914 in O1 and O2 using GstLAL data

Regarding the problems in the previous method, we rerun the search by using GstLAL data. The following table shows the GstLAL parameter data regarding the event GW150914 [2]:

Parameter	Value
Mass 1	$47.9M_{\odot}$
Mass 2	$36.5M_{\odot}$
Spin 1 (along z -direction)	0.962
Spin 2 (along z -direction)	-0.900
Chirp mass	$33.8M_{\odot}$

Using similar techniques from the last method, we search through O1 to look for triggers with mass 1 and mass 2 within a certain percentage range of the chirp mass. The objective is to find a distinctive feature for separating possible lensed triggers from the background. Figure 10 - 14 show the results for 10%, 30% and 50% chirp mass range.

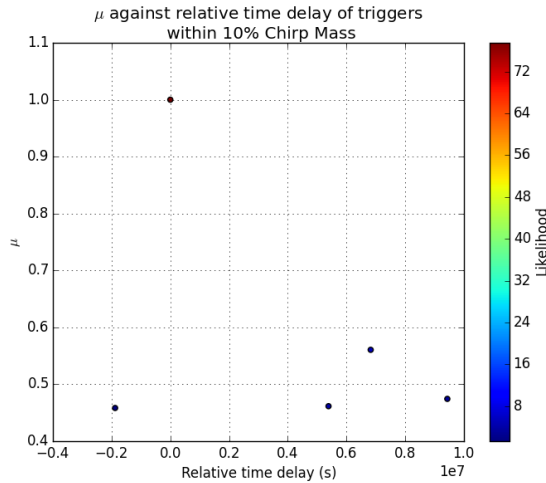


Fig. 10. Searched triggers in O1 with mass 1 and mass 2 within 10% chirp mass range from GW150914.

We note that all of the triggers in the search have likelihood smaller than 20, except for the detected GW150914 event which has a likelihood above 70.

Problems

Although some triggers appear to be distinguishable from the background cluster in the 30% and 50% plots, the magnification of those triggers is unexpectedly high (up to 0.7) considering the exceptionally high SNR of GW150914. A possible reason behind is our neglecting of χ^2 for the detection. We decided to shelve this method and to obtain a distribution of the likelihood of possible lensed triggers as our next step.

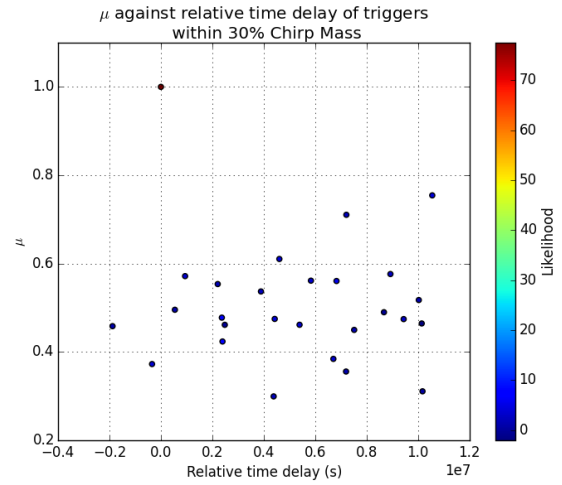


Fig. 11. Searched triggers in O1 with mass 1 and mass 2 within 30% chirp mass range from GW150914.

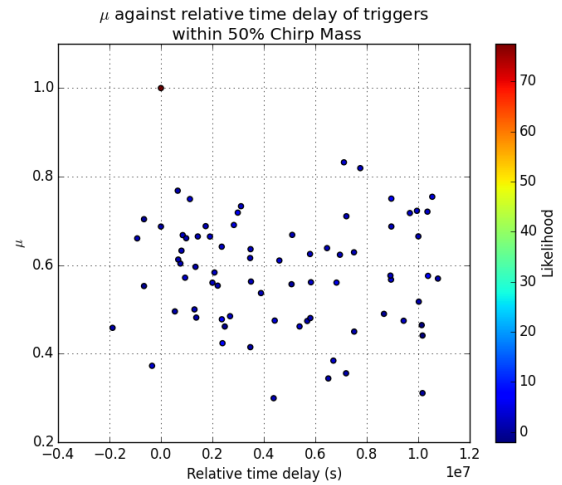


Fig. 12. Searched triggers in O1 with mass 1 and mass 2 within 50% chirp mass range from GW150914.

D. Searching for possible lensed candidates for GW150914 and other events in O1 and O2 using unclustered GstLAL data

We aim to retrieve a likelihood distribution of lensed gravitational wave signals at this stage. The objective of doing so is to figure out the range of search for them. It is expected that the event-count vs ranking statistic threshold curve will be shifted downward for lensed triggers, as shown in Figure 13, since in our GstLAL run, the background noise distribution is not from the entire template bank, but instead from a much smaller template bank, and therefore produces much less background, which allows us to do a targeted search for the lensed gravitational wave signals. This is the major reason why we are launching the injection campaign in the later stage of our project.

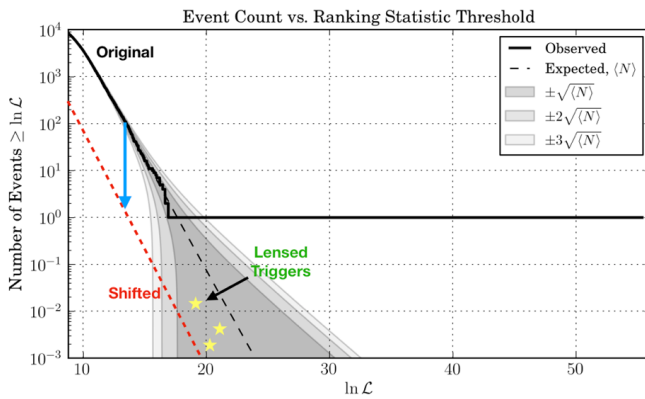


Fig. 13. Expected event-count vs ranking statistic threshold curve for lensed gravitational wave signals, using GW170608 as an example. Note that the shifted red event-count vs ranking statistic threshold curve, and also the yellow stars denoting the lensed triggers we expect to find, are only for illustrative means. In other words, they are not actual data.

We rerun part of the GstLAL run jobs and obtain the unclustered data for each focused event. We then obtain templates around the time of the event and select those with SNR higher than 70% of the maximum. We search through the chunk in which the event happened to find triggers which match the parameters (mass 1, mass2, spin1z, spin2z) in our template bank exactly and regard them as possible lensed triggers. Finally, we plot the distribution of the likelihood of the triggers and compare it with the event-count vs ranking statistic threshold graph. Figure 13 - 16 show the results for GW150914, GW170608 and GW170814. In each of the figure, one sees the solid black line (observed) and the dashed line (expected) indicating the event-count vs ranking statistics threshold curve with the background from the entire template bank. The curve with background from the much smaller template banks we used for our search is not yet to be known. The blue bar(s) in the middle and/or right side of each graph corresponds to the detected event, while those on the left refer to some found triggers with very low likelihood from our search. We hope to get a sense of how the likelihood distribution for lensed gravitational wave signals would look like from

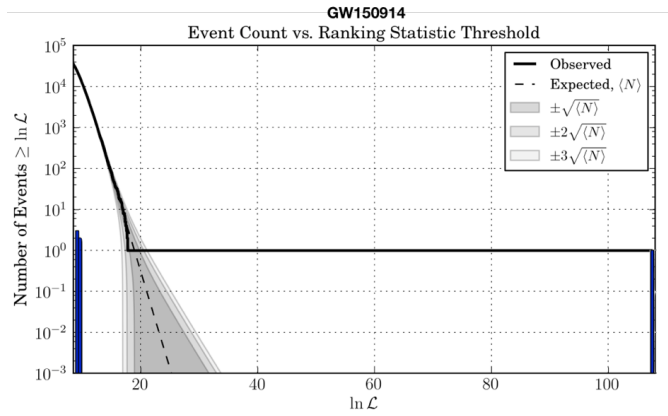


Fig. 14. Distribution of likelihood (blue bars) of searched matching triggers in O1-chunk1 using raw data for the event GW150914. Note that the barely visible blue bar on the right boundary corresponds to the detection of the event GW150914.

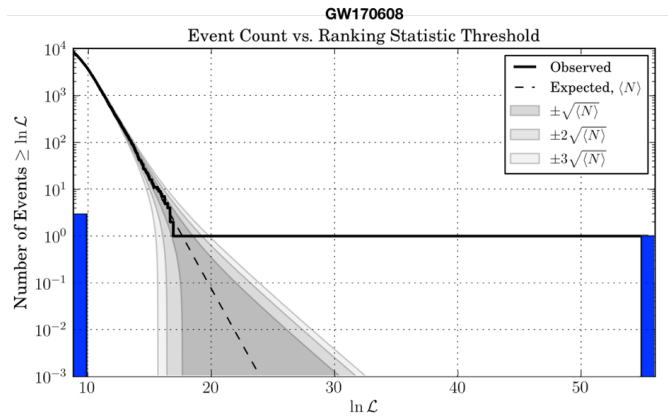


Fig. 15. Distribution of likelihood (blue bars) of searched matching triggers in O2-chunk-GW170608 using raw data for the event GW170608. The blue bar on the right boundary corresponds to the detection of the event GW170608.

these searches.

Problems

From the plots, we can already get a sense of how the distribution of the likelihood of possible lensed triggers will be. However, we are still uncertain about the searching range for possible lensed triggers. Until now, we are still varying the SNR percentage threshold to get a satisfactory result. Therefore, a more systematic way to actually obtain the likelihood distribution of lensed candidates will be to run an injection campaign, which is done in Week 4 - 6.

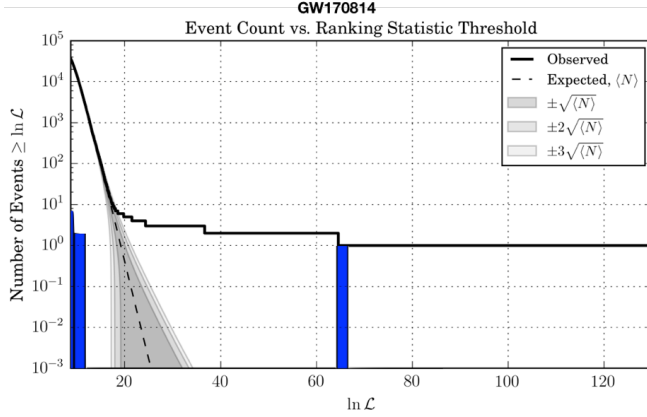


Fig. 16. Distribution of likelihood (blue bars) of searched matching triggers in O2-chunk21 using raw data for the event GW170814. The blue bar in the middle refers to the detection of the event GW170814. Note that the solid (observed) event-count versus ranking statistics threshold curve extends beyond the middle blue bar instead of stopping there, since there is another detection, which is GW170817, in the same chunk we are analysing here.

IV. Work Updates

A. Preparing to run an injection campaign

Following the last part of the previous section, we attempt to run an injection campaign to obtain a likelihood distribution of lensed gravitational wave signals. The first step is to read in the LALInference posterior samples [24]. Table 1 below shows the important items in each of the LALInference posterior sample file (using GW150914 - allSsp_post.dat as a sample).

TABLE I
A TABLE SHOWING THE IMPORTANT ELEMENTS IN EACH OF THE LALINFERENCE POSTERIOR SAMPLE FILE.

Item	Content [25]
l1_end_time	Reference time at Livingston site (time of coalescence / peak amplitude)
v1_end_time	Reference time at VIRGO site (time of coalescence / peak amplitude)
h1_end_time	Reference time at Hanford site (time of coalescence / peak amplitude)
time	Reference time at geocentre (time of coalescence / peak amplitude)
m1	Mass of the primary object (detector frame)
m2	Mass of the secondary object (detector frame)
a1z	The z-component of spin of the primary object
a2z	The z-component of spin of the secondary object
mc	Chirp mass (detector frame)
distance	Distance to source
dec	Declination of the gravitational wave source
ra	Right ascension of the gravitational wave source
psi	Polarisation angle (3 rd Euler angle) required to transform the tensor perturbation in the radiation frame to the detector frame
costheta_jn	Cosine of the angle between the total angular momentum and the line of sight vector
theta_jn	Angle between total angular momentum and line of sight
eta	Symmetric mass-ratio
optimal_snr	Optimal Signal-to-Noise Ratio (SNR) of the model
logl	Natural log of the likelihood
lal_amporder	Post Newtonian amplitude order

Next, we try to make an injection file with a sim_inspirial table containing simulated lensed signals of GW150914 which we produced from the posterior samples. The transfer of information from the posterior samples to the generated sim_inspirial table is not straightforward and some items require re-calculations. The technical details may be found in the attached code files. Table 2 lists the important items in the sim_inspirial table and the related posterior samples' items.

TABLE II
A TABLE SHOWING THE IMPORTANT ELEMENTS IN SIM_INSPIRIAL TABLE AND THE RELATED POSTERIOR SAMPLES' ITEMS.

Item	Content and related posterior samples items
h_end_time	Reference time at Hanford site (time of coalescence / peak amplitude) [Integral value] Related item(s) : h1_end_time
h_end_time_ns	Reference time at Hanford site (time of coalescence / peak amplitude) [Nanosecond] Related item(s) : h1_end_time
l_end_time	Reference time at Livingston site (time of coalescence / peak amplitude) [Integral value] Related item(s) : l1_end_time
l_end_time_ns	Reference time at Livingston site (time of coalescence / peak amplitude) [Nanosecond] Related item(s) : l1_end_time
v_end_time	Reference time at Virgo site (time of coalescence / peak amplitude) [Integral value] Related item(s) : h1_end_time
v_end_time_ns	Reference time at Virgo site (time of coalescence / peak amplitude) [Nanosecond] Related item(s) : h1_end_time
geocent_end_time	Reference time at geocentre (time of coalescence / peak amplitude) [Integral value] Related item(s) : time
geocent_end_time_ns	Reference time at geocentre (time of coalescence / peak amplitude) [Nanosecond] Related item(s) : time
mass1	Mass of the primary object (detector frame) Related item(s) : m1
mass2	Mass of the secondary object (detector frame) Related item(s) : m2
mchirp	Chirp mass (detector frame) Related item(s) : mc
spin1z	The z-component of spin of the primary object Related item(s) : a1z
spin2z	The z-component of spin of the secondary object Related item(s) : a2z
distance	Distance to source Related item(s) : distance, ra, dec, optimal_snr
longitude	Right ascension* of the gravitational wave source Related item(s) : ra
latitude	Declination* of the gravitational wave source Related item(s) : dec
eta	Symmetric mass-ratio Related item(s) : eta
inclination	angle between total angular momentum and line of sight Related item(s) : theta_jn
polarization	Polarisation angle (3 rd Euler angle) required to transform the tensor perturbation in the radiation frame to the detector frame Related item(s) : psi
amp_order	Post Newtonian amplitude order Related item(s) : lal_amporder

Following [26], the quantity

$$\rho(t) = \frac{|z(t)|}{\sigma} \quad (19)$$

is the amplitude signal-to-noise ratio of the (quadrature) matched filter, where σ is a measure of the sensitivity of the instrument defined by

$$\sigma^2 = 4 \int_0^\infty \frac{\tilde{h}_1(f)}{S(f)} df \quad (20)$$

with \tilde{h}_1 being the signal and $S(f)$ being the power spectral density, and

$$z(t) = 4 \int_0^\infty \frac{\tilde{s}(f)[\tilde{h}_1^*(f)]}{S(f)} e^{2\pi i f t} df \quad (21)$$

is the modulus of the complex filter output, with $s(f)$ following the definition in equation (1). With such, a biased estimate of the **effective distance** to the candidate system is

$$D_{\text{eff}} = \left(\frac{\sigma}{\rho}\right) \text{Mpc}. \quad (22)$$

We generate simulated lensed signals by altering the effective distance of the samples with equation (18).

Problems

A challenge to generating simulated lensed signals is that the samples store only "distance" D instead of "effective distance" D_{eff} , and both of them depend on the sky location (i.e. right ascension α and declination δ) of the source. Particularly, the relationship between D and D_{eff} is given by

$$D_{\text{eff}} = D \left[F_+^2 \left(\frac{1 + \cos^2 \iota}{2} \right)^2 + F_\times^2 \left(\cos^2 \iota \right) \right]^{-\frac{1}{2}}, \quad (23)$$

where F_+ and F_\times are the antenna response functions for the signal. The resolution to this is to make use of the *ComputeDetAMResponse* from the *lal* python package to compute the values of F_+ and F_\times . For the full computational code, please refer to the attachment.

B. Running the injection campaign

We substitute information (mass1, mass2, spin1z, spin2z, distance) of the original injection file by those of our simulated lensed signals. Using the modified injection file, we rerun the GstLAL run to search for the injected lensed signals. Currently we are running a full GstLAL run for Observation Run 1, chunk 5 for the event GW150914 on the CIT cluster and the figure below shows the distance at which you should see a lensed signal for GW150914. The first panel shows the time evolution of the horizon distance and the second panel shows the same information in histogram form.

Note that when we generate simulated lensed signals, we **choose to**constrained the SNR of each signal to have a

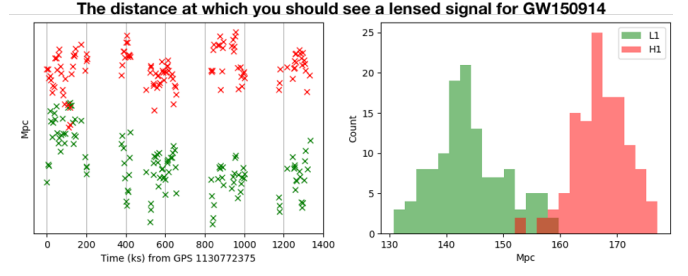


Fig. 17. The distance at which you should see a lensed signal for GW150914.

minimum SNR of 4. For each sample, within the range of SNR 4 to the original SNR of the sample, we generate 10 templates with SNR uniformly distributed in the range by altering their effective distances. From equation (22) we see that

$$\rho \propto \frac{1}{D_{\text{eff}}}, \quad (24)$$

and hence by altering the SNR ρ of the signal we have

$$d\rho \propto \frac{dD_{\text{eff}}}{D_{\text{eff}}^2}. \quad (25)$$

This relationship is reflected from the histogram shown on the right side of Figure 18. If we choose another way to generate our simulated signals, for instance,

$$\rho^2 \propto \frac{1}{D_{\text{eff}}}, \quad (26)$$

the distribution shown in the histogram will be different.

Problems

The clusters have been problematic and slow over the time we are running the injection campaign. There are moments when we cannot even log-into the clusters. According to the people managing the clusters, they are either encountering internet issues or hardware issues. We also suspect that the problems are attributed to the current integration of KAGRA members into the clusters. To resolve the problem, we try to do a shortcut GstLAL run by reducing the injection time range from the full observation chunk to a week time. We are currently using this approach for the detected event GW151226. We expect this will help to make the jobs complete quicker. Although the result may not be perfect, it will still be decent and satisfactory.

C. Literature review on gravitational lensing of gravitational waves

If lensed gravitational wave signals can be successfully detected, we will go on and try to infer some properties of the gravitational lens, including its mass, the lens-observer distance, and the lens-source distance. We try to follow the mathematics and approach of [27] to compute the probability distribution of relative time delays and magnification of

lensed gravitational wave signals through a singular isothermal ellipsoid (SIE) lens model.

Singular isothermal ellipsoid (SIE) lens models have a surface mass density which diverges at the center. These lenses can produce either two or four images. The lens model itself has two parameters, namely the velocity dispersion σ and the axis-ratio q . We follow [27] to generate these parameters with distribution taken from the SDSS galaxy population.

The following figures shows the reproduced results (Figure 20 and 21) compared to the original results shown in [27] (Figure 18 and 19).

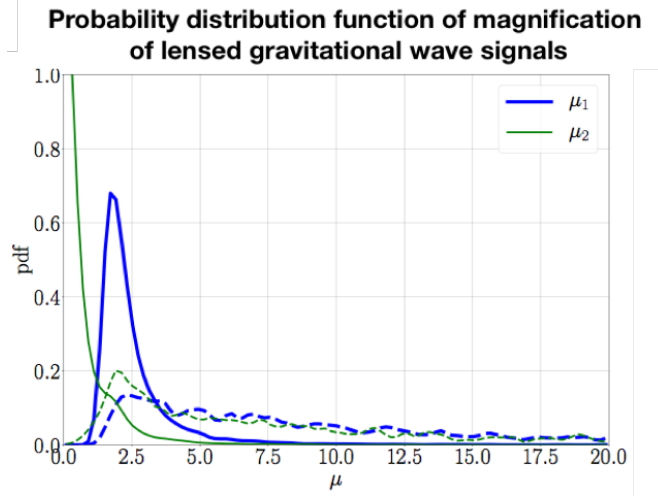


Fig. 18. Probability distribution function of magnification μ_1 and μ_2 of the two dominant lensed gravitational wave signals as shown in [27]. Here, we only reproduce the result for μ_2 . The Solid (dashed) traces show distributions before (after) applying the detection threshold $\text{SNR} > 8$. The component masses of the simulated events are sampled from power law 1 distribution.

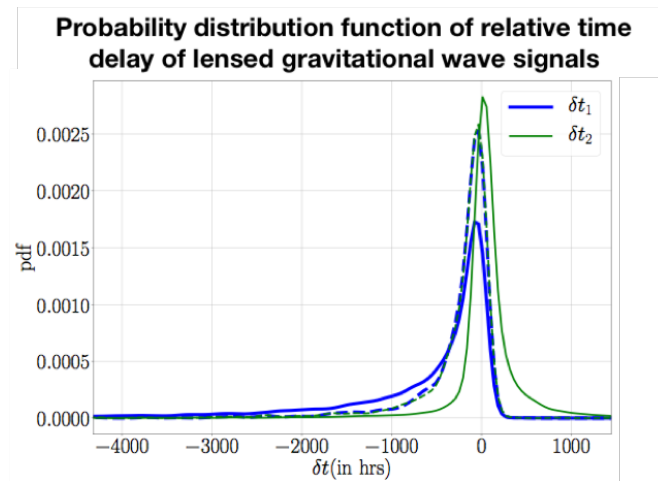


Fig. 19. Probability distribution function of relative time delay δt_1 and δt_2 of the two dominant lensed gravitational wave signals as shown in [27]. Here, we only try reproduce the result for δt_2 dashed. The Solid (dashed) traces show distributions before (after) applying the detection threshold $\text{SNR} > 8$. The component masses of the simulated events are sampled from power law 1 distribution.

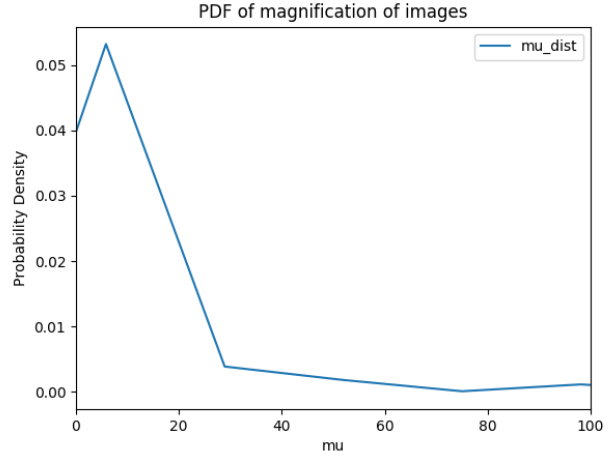


Fig. 20. Probability distribution function of magnification of lensed gravitational wave signals reproduced. Here, we only reproduce the result for μ_2 dashed. Note that our reproduced results does not go to 1.0 at $\mu = 0$, since we have taken absolute value for negative magnifications.

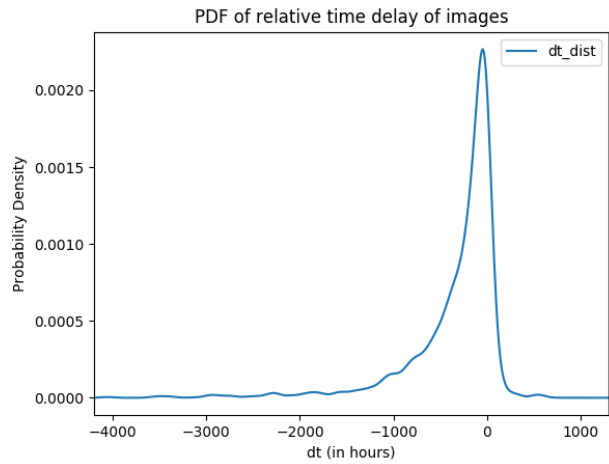


Fig. 21. Probability distribution function of relative time delay δt of lensed gravitational wave signals reproduced. Here, we only reproduce the result for δt_2 dashed.

We take a step further to plot the 2D contour plot of the probability distribution of both the relative time delay and magnification of lensed gravitational signals, as shown in Figure 22.

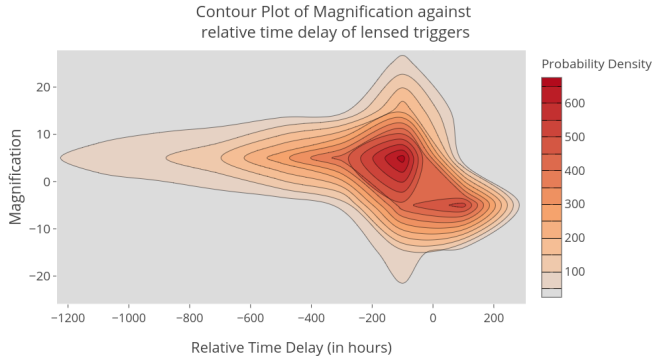


Fig. 22. Probability distribution function of relative time delay δt of lensed gravitational wave signals reproduced. Here, we only reproduce the result for δt_2 dashed.

We will go on in the coming weeks to research on the probability distribution of relative time delay and magnification of lensed gravitational wave signals under different lens models.

Problems

We have reproduced a nearly identical probability distribution function of relative time delay δt of lensed gravitational wave signals as shown in [27]. The magnification distribution we reproduce is not satisfactory. We suspect that the reason behind is we do not take magnification < 0 into account when we produce the distribution. There is no related discussion about negative magnification in [27]. We will go on to look for more research paper for reference and to investigate the meaning of negative magnification in this context in the coming weeks, and try to reproduce again the result shown in [27]. We will also try to approach the researchers of [27] and see if we can collaborate on this project.

V. Plans and foreseeable challenges

A. Inferring the properties of the gravitational lens

Once we identify lensed gravitational wave signals, we will go on and try to infer some properties of the gravitational lens, including its mass, the lens-observer distance and the lens-source distance.

Foreseeable challenge(s)

The parameters inference step requires further literature review on gravitational lensing and involves more calculations. Alternatively, we may try to use available lens models, like in Section V we follow [27] to reproduce the results for probability distribution of relative time delay and magnification of lensed gravitational wave signals under the influence of a singular isothermal ellipsoid, to check how likely the identified triggers are under the effect of the proposed models. We may also consider making use of the package LENSTOOLS [28]. The package is being widely used for lens optimisation in studying gravitational lensing but requires further literature review before it can be applied to our research.

B. Running injection campaign for all other detected events

If the current injection campaigns for GW150914 and GW151226 succeed, we will go on to run injection campaign for other detected events such as GW170104 and GW170608.

Foreseeable challenge(s)

The clusters are still unstable and slow. Therefore, the injection campaign may take more time than expected.

C. Using galaxy cluster / supercluster catalogue

We may try to make use of the available galaxy cluster / supercluster catalogue to verify the presence of possible gravitational lens between the detectors and the source once lensed gravitational wave signals are identified.

Foreseeable challenge(s)

The catalogues available in the present only covers a small region of the sky. It is possible that the gravitational wave source is not in the covered region. We have to check the coverage of catalogues to see if they are applicable to our research.

D. Pipelining the search for lensed gravitational wave signals

To make the search for gravitational wave signals efficient, we may try to construct a pipeline (makefile) for the search. This can make the process more time-efficient, and it will also make error-shooting easier.

Foreseeable challenge(s)

Regarding my unfamiliarity towards pipeline and makefile construction, more literature review has to be conducted before making the pipeline for the lensed gravitational wave signals search.

E. Re-introducing the sky location problem to the project

At this stage of our project, we have neglected the alteration in sky location of the source when we inject simulated lensed signals using LALInference posterior samples. In particular, we need to investigate the range of sky location to search for lensed gravitational wave signal, instead of using the range suggested by LALInference. Figure 24 illustrates the problem.

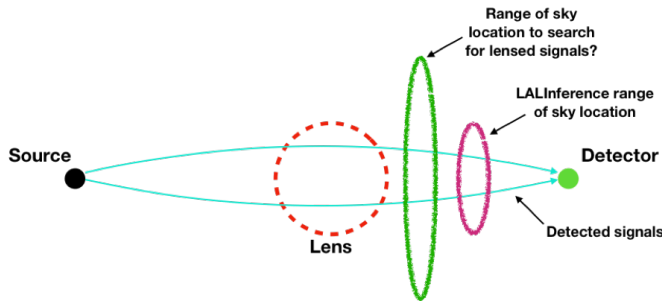


Fig. 23. An illustration of the sky-location problem on the project.

We may also try to find the correlation between the relative time delay δt of lensed gravitational wave signals and the corresponding sky-location of the source (i.e. right ascension α and declination δ), or even trace the lensed gravitational wave signals.

Foreseeable challenge(s)

This part is rather time-consuming and may not be finished in the coming few weeks. It will be carried on after the SURF period.

VI. Work Plan

1) Pre-Surf Period:

- Literature review on gravitational lensing, gravitational wave data analysis and related mathematics
- Construct models for lensed gravitational wave signals
- Complete the mathematical formulation for the SNR, FAR and related data analysis for this research
- Learn how to run a GstLAL search
- Run template searches on the drafted models to observe the effect, and modify them in accordance.

2) SURF Period:

- 19 June, 2018 : Arrive at Caltech
- 19 June - 9 July, 2018 [Week 1-3] :
 - (i) Complete the follow-up work during the Pre-Surf Period
 - (ii) Rerun searches using the modified models
 - (iii) Analyse the results and suggest further modifications on the models
- 10 July, 2018 : First Interim Report to be submitted
- 11 July - 20 July, 2018 [Week 4-5] :
 - (i) Run injection campaign
 - (ii) Analyse the results
- 21 July - 2 August, 2018 [Week 5-7] :
 - (i) Run injection campaign
 - (ii) Analyse the results
 - (iii) Start preparing the second interim report and the final paper
- 3 August 2018 : Second Interim Report to be submitted
- 4 August - 17 August, 2018 [Week 7-9] :
 - (i) Attempt to infer the properties of the lens
 - (ii) Pipeline the search process
 - (iii) Preparation of final presentation and final paper

- 23 - 24 August 2018 : Summer Seminar Days

3) Post Surf Period:

- 24 August 2018 : Returning to Hong Kong
- Complete final paper
- Follow-up work on the summer research
- Continue related research in gravitational wave science

REFERENCES

- [1] Albert Einstein. *The Meaning of Relativity*. -, 1922.
- [2] B.P. Abbott. Observation of gravitational waves from a binary black hole merger. *Phys. Rev. Lett.*, 166, 2016.
- [3] B.P. Abbott et al. (LIGO Scientific Collaboration and Virgo Collaboration). Gw151226: Observation of gravitational waves from a 22-solar-mass binary black hole coalescence. *Phys. Rev. Lett.*, 116, 2016.
- [4] B.P. Abbott et al. (LIGO Scientific and Virgo Collaboration). Gw170104: Observation of a 50-solar-mass binary black hole coalescence at redshift 0.2. *Phys. Rev. Lett.*, 118, 2017.
- [5] B. P. Abbott, R. Abbott, T. D. Abbott, F. Acernese, K. Ackley, C. Adams, T. Adams, P. Addesso, R. X. Adhikari, and V. B. Adya. Gw170608: Observation of a 19 solar-mass binary black hole coalescence. *The Astrophysical Journal Letters*, 851(2), 2017.
- [6] B.P. Abbott et al. (LIGO Scientific Collaboration and Virgo Collaboration). Gw170814: A three-detector observation of gravitational waves from a binary black hole coalescence. *Phys. Rev. Lett.*, 119, 2017.
- [7] B. P. Abbott et al. (LIGO Scientific Collaboration and Virgo Collaboration). Gw170817: Observation of gravitational waves from a binary neutron star inspiral. *Phys. Rev. Lett.*, 119, 2017.
- [8] Albert Einstein and M. Grossmann. Kovarianzeigenschaften der feldgleichungen der auf die verallgemeinerte relativitätstheorie gegründeten gravitationstheorie. *Zeitschrift für Mathematik und Physik*, 63:215–225, 1915.
- [9] James Hartle. *Gravity - An Introduction to Einstein's General Relativity*. Pearson Education, 2003.
- [10] Albert Einstein. Näherungsweise integration der feldgleichungen der gravitation. *Preussische Akademie der Wissenschaften, Sitzungsberichte*, pages 688–696, 1916.
- [11] LIGO-Scientific-Collaboration, Virgo-Collaboration, Fermi-Gamma-Ray-Burst-Monitor, and INTEGRAL. Gravitational waves and gamma-rays from a binary neutron star merger: Gw170817 and grb 170817a. *The Astrophysical Journal Letters*, 848, 2017.
- [12] Tjonnie G. F. Li. *Extracting Physics from Gravitational Waves*. Springer International Publishing, 2015.
- [13] <https://www.ligo.caltech.edu/>.
- [14] B.S. Sathyaprakash and B.F. Schutz. Physics, astrophysics and cosmology with gravitational waves. *Living Rev. Relativity*, 2, 2009.
- [15] B P Abbott, R Abbott, T D Abbott, M R Abernathy, F Acernese, K Ackley, M Adamo, C Adams, T Adams, and P Addesso. Characterization of transient noise in advanced ligo relevant to gravitational wave signal gw150914. *Classical and Quantum Gravity*, 33(13), June 2016.
- [16] Drew Garvin Keppel. *Signatures and dynamics of compact binary coalescences and a search in LIGO's S5 data*. PhD thesis, California Institute of Technology, 2009.
- [17] Ramesh Narayan and Matthias Bartelmann. Lectures on gravitational lensing. -, 1997.
- [18] Steven T. Myers. Scaling the universe: Gravitational lenses and the hubble constant. *Proc. Natl. Acad. Sci. USA*, 1999.
- [19] Ryuichi Takahashi. Arrival time differences between gravitational waves and electromagnetic signals due to gravitational lensing. *ApJ*, 835, 2016.
- [20] Ehlers J.-Falco E.E. Schneider, P. *Gravitational Lenses*. Springer International Publishing, 1992.
- [21] Ryuichi Takahashi and Takashi Nakamura. Wave effects in gravitational lensing of gravitational waves from chirping binaries. *Astrophys.J.*, 593:1039–1051, 2003.
- [22] C. Messick, K. Blackburn, P. Brady, P. Brockill, K. Cannon, R. Cariou, S. Caudill, S. J. Chamberlin, J. D. E. Creighton, R. Everett, C. Hanna, D. Keppel, R. N. Lang, T. G. F. Li, D. Meacher, A. Nielsen, C. Pankow, S. Privitera, H. Qi, S. Sachdev, L. Sadeghian, L. Singer, E. G. Thomas, L. Wade, M. Wade, A. Weinstein, and K. Wiesner. Analysis framework for the prompt discovery of compact binary mergers in gravitational-wave data. , 95(4):042001, February 2017.
- [23] John Veitch, Vivien Raymond, Benjamin Farr, Will M. Farr, Philip Graff, Salvatore Vitale, Ben Aylott, Kent Blackburn, Nelson Christensen, Michael Coughlin, Walter Del Pozzo, Farhan Feroz, Jonathan Gair, Carl-Johan Haster, Vicky Kalogera, Tyson Littenberg, Ilya Mandel, Richard O'Shaughnessy, Matthew Pitkin, Carl Rodriguez, Christian Röver, Trevor Sidery, Rory Smith, Marc Van Der Sluys, Alberto Vecchio, Will Voudsen, and Leslie Wade. Robust parameter estimation for compact binaries with ground-based gravitational-wave observations using the lalinference software library. *Phys. Rev. D*, 91, 2015.
- [24] https://git.ligo.org/pe_event_samples.
- [25] <https://www.lsc-group.phys.uwm.edu/>.
- [26] Bruce Allen, Warren G. Anderson, Patrick R. Brady, Duncan A. Brown, and Jolien D. E. Creighton. Findchirp: An algorithm for detection of gravitational waves from inspiraling compact binaries. *Phys. Rev. D*, 85(12), June 2012.
- [27] K. Haris, Ajit Kumar Mehta, Sumit Kumar, Tejaswi Venumadhav, , and Parameswaran Ajith. Identifying strongly lensed gravitational wave signals from binary black hole mergers. -, 2018.
- [28] Andrea Petri. Mocking the weak lensing universe: the lenstools python computing package. *Astronomy Computing*, 17:73–79, October 2016.